



Contents lists available at ScienceDirect

Journal of Wind Engineering & Industrial Aerodynamics

journal homepage: www.elsevier.com/locate/jweia

A new Gaussian-based analytical wake model for wind turbines considering ambient turbulence intensities and thrust coefficient effects

Takeshi Ishihara, Guo-Wei Qian*

Department of Civil Engineering, School of Engineering, The University of Tokyo, 7-3-1, Hongo, Bunkyo-ku, Tokyo, Japan

ARTICLE INFO

Keywords:

wind turbine wake
Large eddy simulation
Wake model
Ambient turbulence intensity
Thrust coefficient

ABSTRACT

A new wake model for wind turbines considering ambient turbulence intensity and thrust coefficient effects is proposed by numerical and analytical studies. Firstly, two kinds of operating condition with different thrust coefficients under two types of inflow with different ambient turbulence intensity are simulated for a model and a utility-scale wind turbine by using large eddy simulation (LES). The predicted mean velocity and turbulence intensity in the wakes of two wind turbines are compared with those obtained from the wind tunnel tests to validate numerical models. Subsequently, a new wake model is proposed to predict the mean velocity and turbulence intensity distribution in the wake regions of wind turbines. The model is derived based on the axial symmetry and self-similarity assumption for wake deficit and added turbulence intensity. All parameters of the proposed model are determined as the function of ambient turbulence intensity and thrust coefficient identified based on the various large eddy simulations. The velocity deficit and added turbulence intensity in the wake predicted by the new wake model show good agreement with the LES simulations and experimental results in the near and far wake regions.

1. Introduction

Wind turbines in a wind farm operating in the downwind wake flow are subjected to two main problems: decreased energy production due to the velocity deficit and increased fatigue loading due to the added turbulence intensity generated by the upwind turbine (Vermeer et al., 2003; Barthelmie et al., 2009). Especially in the offshore wind farm, where the ambient turbulence intensity is lower than that in the terrestrial boundary layer, the wakes recover more slowly and bring severer effects (Ishihara et al., 2004; Wu and Porté-Agel, 2012). Therefore, an accurate evaluation of the wake effect is essential in the wind farm layout design in order to improve the power efficiency and the lifetime of the turbine.

Prediction of wake effect requires detailed understanding of the behavior of wake flow and its interaction with atmospheric boundary layer. In previous studies, the wake characteristics in the atmospheric boundary layer have been investigated by wind tunnel tests (Ishihara et al., 2004; Chamorro and Porté-Agel, 2009), however it is difficult to capture the detailed turbulence structure due to the constraint of measurement.

In recent years, computational fluid dynamics (CFD) has been used to study wind turbine wake flow and to optimize wind farm layout

(Sanderse et al., 2011). In these studies, the large-eddy simulation (LES) was popularly used for the study of wind turbine wake characteristics, and the wind turbine induced forces were modelled using either of the two approaches, the generalized actuator disk model (ADM) or actuator line model (ALM). The ALM is used to reproduce detailed three-dimensional rotational effects, like tip vortices. However, it is noted that finer mesh and smaller time steps are required for ALM, thus this method is costly for LES simulation of a large wind farm. According to the study in reference (Witha et al., 2014), the CPU time of ALM simulation is greatly enhanced compared to the ADM simulation by a factor of 4–12 depending on the grid resolution. The earliest version of ADM is the actuator disk model without rotation (ADM-NR), in which the turbine induced force is parameterized as an overall thrust force uniformly acting on the rotor disk (Jiménez et al., 2007; Calaf et al., 2010; Goit and Meyers, 2015). Another extended ADM uses the blade element momentum (BEM) theory (Burton et al., 2011) to calculate the lift and drag forces and then unevenly distribute them on the actuator disk. This modified approach is referred to as the actuator disk model with rotation (ADM-R). The ADM-R has been employed in LES simulation and validated by the wind tunnel tests for the wind turbine wakes in turbulent boundary layers (Wu and Porté-Agel, 2011, 2012). Although the detailed

* Corresponding author.

E-mail address: qian@bridge.t.u-tokyo.ac.jp (G.-W. Qian).<https://doi.org/10.1016/j.jweia.2018.04.010>

Received 18 August 2017; Received in revised form 25 November 2017; Accepted 9 April 2018

characteristics of mean velocity and turbulence in the turbine wake have been examined in these studies (Wu and Porté-Agel, 2011; Xie and Archer, 2014), the effect of ambient turbulence intensity and thrust coefficient require further systematic investigation.

In comparison to wind tunnel tests and numerical simulations, wake models have advantages in designing and optimizing wind farm layout because of its simplicity and high efficiency (Crespo et al., 1999). The wake can be generally divided into near wake region and far wake region (Vermeer et al., 2003). The near wake region typically has a length less than three diameters downwind the turbine (Crespo and Hernández, 1996), which is complicated to cope with due to the fact that it is significantly affected by the blade aerodynamics, stalled flow, tip vortices as well as nacelle and tower (Vermeer et al., 2003; Xie and Archer, 2014). Thus, most wake modelling mainly focus on the far wake region, where the wake is fully developed and the velocity deficit and the added turbulence intensity can be assumed axisymmetric and have self-similar distributions in the wake cross-sections (Vermeer et al., 2003).

Prediction of the velocity deficit is the primary objective of wake models. One of the classical and widely used wake model for velocity deficit was proposed by Jensen (1983), and was developed further by Katic et al. (1986), which assumes a linearly expanding wake with a uniform profile, termed “a top-hat shape”, for the velocity deficit. The Katic et al.’s model only considers the mass conservation. More recently Frandsen (Frandsen et al., 2006) proposed a model that applied the balance of momentum in addition to the mass conservation. It still took a top-hat assumption for the velocity deficit. In comparison with the top-hat assumption, Gaussian distribution is more reasonable for the velocity deficit profile in wake cross section, which was derived by Ishihara et al. (2004) and observed in the experimental data (Ishihara et al., 2004; Chamorro and Porté-Agel, 2009) and numerical simulations (Xie and Archer, 2014). It was also employed in several wake models (Ishihara et al., 2004; Ainslie, 1988; Bastankhah and Porté-Agel, 2014; Gao et al., 2016). However, there are still problems of robustness and universality for these models.

Modelling the turbulence in wind turbine wake flows is also important since the wake induced turbulence increases the fatigue loading of the downwind turbine. Considering the complex nature of turbulence, it is common to model the maximum added turbulence intensity $\Delta I_{1\max}$, which normally occurs at the top tip height level. Based on the measurement data, Quarton and Ainslie (1989) proposed a widely used empirical expression for $\Delta I_{1\max}$, which is proportional to thrust coefficient and ambient turbulence intensity. The distance from wind turbine was normalized by the estimated near wake length x_N defined by Vermeulen (1980). The parameters in Quarton’s model were modified by Hassan (Hassan et al., 1990) based on wind tunnel measurements. Crespo and Hernández (1996) proposed a similar model for $\Delta I_{1\max}$, which is related to the induction factor and ambient turbulence intensity. These three wake models are quite similar and show overestimation in the near wake region. In addition, the distribution of added turbulence intensity in the wake cross section is also important in the wind farm layout design and has not been investigated yet.

In this paper, a new wake model for wind turbines is proposed to consider the ambient turbulence intensity and thrust coefficient effects by numerical and analytical studies. In section 2, the numerical model used in this study is described and the systematic simulations are conducted and compared with the experimental data. Section 3 presents a new wake model proposed in this study. The accuracy of the proposed model and the conventional wake models are examined by the LES simulations and the wind tunnel tests. Finally, conclusions of this study are summarized in section 4.

2. Numerical model and validation

In this study, LES is employed to simulate the wind turbine wake flows, and the governing equations are presented in section 2.1. The accuracy of the wind turbine model is validated in section 2.2 by

comparing the calculated thrust coefficients with the measured data of a model and a utility-scale wind turbine, respectively. Section 2.3 describes the set-up of the numerical simulations, including the computational domain and the main parameters used in each case. The turbulent inflows generated in the numerical wind tunnel are validated in section 2.4. Finally, the characteristics of the mean velocity and turbulence intensity in the wake region under different conditions are investigated and validated by the wind tunnel test in section 2.5.

2.1. Governing equations

In the LES, large eddies are directly computed, while the influences of eddies smaller than grid spacing are parameterized. The Boussinesq hypothesis is employed, and the Smagorinsky-Lilly model (Smagorinsky, 1963) is used to calculate the subgrid-scale (SGS) Reynolds stress.

The governing equations are filtered incompressible Navier-Stokes equations and are expressed as (Ferziger and Perić, 2002):

$$\frac{\partial \rho \tilde{u}_i}{\partial x_i} = 0 \quad (1)$$

$$\frac{\partial}{\partial t} (\rho \tilde{u}_i) + \frac{\partial}{\partial x_j} (\rho \tilde{u}_i \tilde{u}_j) = \frac{\partial}{\partial x_j} \left(\mu \frac{\partial \tilde{u}_i}{\partial x_j} \right) - \frac{\partial \tilde{p}}{\partial x_i} - \frac{\partial \tau_{ij}}{\partial x_j} + f_i \quad (2)$$

where \tilde{u}_i and \tilde{p} are respectively filtered velocities and pressure, ρ is the air density, μ is the dynamic viscosity, f_i is the source term to present the external force corresponding to the effects of the wind turbine on the momentum, and τ_{ij} is the SGS stress, which is modelled as:

$$\tau_{ij} = -2\mu_t \tilde{S}_{ij} + \frac{1}{3} \tau_{kk} \delta_{ij} \quad (3)$$

where μ_t denotes SGS turbulent viscosity, δ_{ij} is the Kronecker delta and \tilde{S}_{ij} is the rate-of-strain tensor for the resolved scale which is defined as follows:

$$\tilde{S}_{ij} \equiv \frac{1}{2} \left(\frac{\partial \tilde{u}_i}{\partial x_j} + \frac{\partial \tilde{u}_j}{\partial x_i} \right) \quad (4)$$

Smagorinsky-Lilly model is used for the SGS turbulent viscosity, i.e.:

$$\mu_t = \rho L_S^2 |\tilde{S}| = \rho L_S^2 \sqrt{2\tilde{S}_{ij}\tilde{S}_{ij}} \quad (5)$$

where L_S denotes the mixing length for subgrid-scales and it is calculated by:

$$L_S = \min(\kappa\delta, C_S V^{1/3}) \quad (6)$$

κ is the von Karman constant, 0.42, δ is the distance to the closet wall and V is the volume of a computational cell. In this study, Smagorinsky constant C_S is determined as 0.032 based on the study performed by Oka and Ishihara (2009).

For the wall-adjacent cells, the wall shear stresses are obtained from the laminar stress-strain relationship in laminar sublayer:

$$\frac{\tilde{\mu}}{\mu_\tau} = \frac{\rho \mu_\tau y}{\mu} \quad (7)$$

Provided that the mesh cannot resolve the laminar sublayer, the centroid of the wall-adjacent cells is assumed to fall within the logarithmic region of the boundary layer, and then the law of the wall is employed as follows:

$$\frac{\tilde{\mu}}{\mu_\tau} = \frac{1}{\kappa} \ln E \left(\frac{\rho \mu_\tau y}{\mu} \right) \quad (8)$$

where $\tilde{\mu}$ is the filtered velocity tangential to the wall, y is the distance between the center of the cell and the wall, μ_τ is friction velocity, and the

constant E is 9.793.

Finite volume method is employed and the simulations are performed with ANSYS FLUENT. The second order central difference scheme is used for the convective and viscosity term, and the second implicit scheme is adopted for the unsteady term. SIMPLE (semi-implicit pressure linked equations) algorithm is employed for solving the discretized equations (Ferziger and Perić, 2002). The simulation time is 12 s and the later 10 s is used for the average.

2.2. Wind turbine model

In this study, the ADM-R model is adopted to determine the rotor-induced forces for a model wind turbine in the wind tunnel test and a utility-scale wind turbine. The model wind turbine is a 1/100 scale model of Mitsubishi's MWT-1000 and the detailed information of the wind tunnel test setup was described by Ishihara et al. (2004) (see Fig. 1). The utility-scale wind turbine model is based on the offshore 2.4 MW wind turbine at the Choshi demonstration site, Japan (see Fig. 2).

The lift and drag forces acting on the turbine blades are calculated by using the blade-element theory. The relation between wind velocity and forces acting on a blade element of length dr located at radius r is shown in Fig. 3, where x and θ denote the axial and tangential directions respectively, α is the angle of attack, β is the local pitch angle and ϕ is the angle between the relative velocity and rotor plane. dF_L and dF_D are the lift and drag forces acting on the blade element and are given by:

$$dF_L = \frac{1}{2} \rho W^2 c C_L dr, \quad dF_D = \frac{1}{2} \rho W^2 c C_D dr \quad (9)$$

where c is the chord length, C_D and C_L are the lift and drag coefficients, respectively. W is the local relative velocity with respect to the blade element and is defined as $W = \sqrt{U_x^2 + (\Omega r - U_\theta)^2}$, where U_x and U_θ are the axial and tangential velocities of the incident flow at the blade. The resulting axial force dF_x and tangential force dF_θ on blade element can be expressed as:

$$dF_x = dF_L \cos \phi + dF_D \sin \phi \quad (10)$$

$$dF_\theta = dF_L \sin \phi - dF_D \cos \phi \quad (11)$$

The force per unit volume in each annular with an area of $\delta A = 2\pi r \delta r$ and a thickness of Δx is expressed by:

$$f_x = \begin{cases} -\frac{B}{2\pi r} \frac{dF_x}{\Delta x \delta r} & 0 \leq x \leq \Delta x, 0 \leq r \leq R \\ 0 & \text{Other} \end{cases} \quad (12)$$

$$f_\theta = \begin{cases} -\frac{B}{2\pi r} \frac{dF_\theta}{\Delta x \delta r} & 0 \leq x \leq \Delta x, 0 \leq r \leq R \\ 0 & \text{Other} \end{cases} \quad (13)$$

where B is the number of blades.

In the blade element momentum (BEM) theory (Burton et al., 2011), the axial and tangential components of the incident flow velocity at blades are assumed as $U_x = U_0(1 - a)$ and $U_\theta = -\Omega r a'$, where U_0 is the free upstream wind speed, Ω is the turbine rotational speed, a and a' are the induction factors in the axial and tangential directions, respectively. They are unknown and solved based on the axial and angular momentum conservations.

In the wind farm simulation, the free upstream wind speed U_0 for a turbine in the farm is not known. Thus, the axial velocity at the rotor disk U_x and a' are selected as the unknown parameters instead of a and a' (Calaf et al., 2010; Goit and Meyers, 2015). In this study, a coupled BEM-CFD method is adopted, in which U_x is directly obtained from the CFD simulation result and the local relative velocity is given as:

$$W = \sqrt{U_x^2 + (\Omega r)^2 (1 + a')^2} \quad (14)$$

where a' is solved based on the angular momentum conservation as shown in the BEM theory:

$$a' = \frac{g_2}{(1 - g_2)}, \quad g_2 = \frac{Bc}{2\pi r} \frac{(C_L \sin \phi - C_D \cos \phi)}{4F_t F_h \sin \phi \cos \phi} \quad (15)$$

where F_t and F_h are the tip loss factor and hub loss factor and calculated by the following equations

$$F_t = \frac{2}{\pi} \arccos \left[\exp \left(-\frac{B}{2} \left(\frac{R}{r} - 1 \right) \sqrt{1 + (\Omega r / U_x)^2} \right) \right] \quad (16)$$

$$F_h = 1.0 \quad (17)$$

An iterative process is used to calculate the tangential induction factors a' , in which the initial value for a' is set to 0 and the convergence tolerance is specified as 1×10^{-4} .

The aerodynamic characteristics of the airfoils datasets of the sample 2 MW offshore wind turbine model provided by GL Garrad Hassan

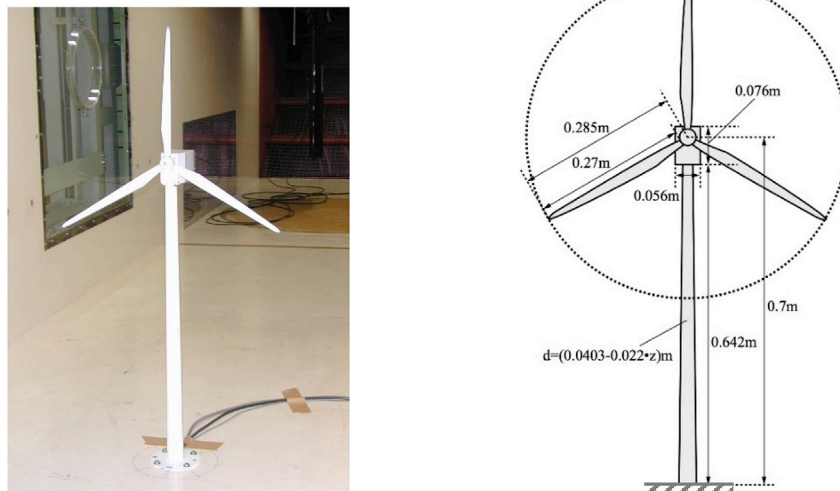


Fig. 1. 1/100 scale model wind turbine in the wind tunnel test and its dimensions.

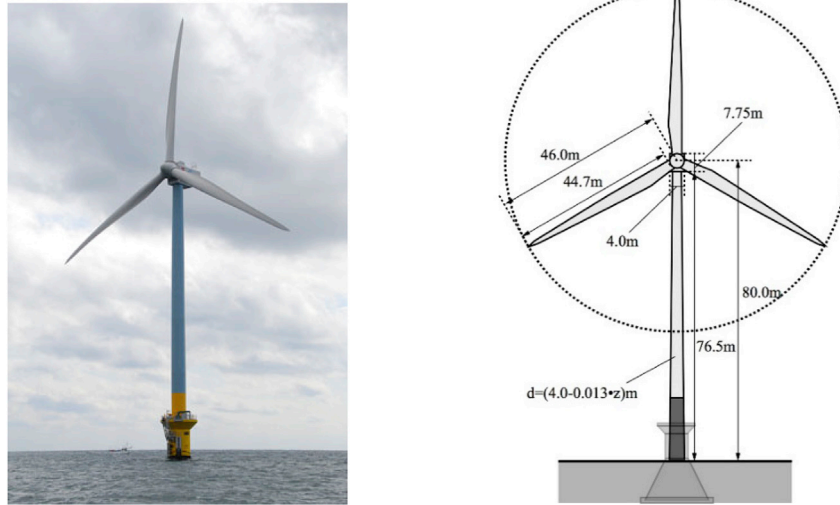


Fig. 2. 2.4 MW wind turbine at Choshi demonstration site and its dimensions.

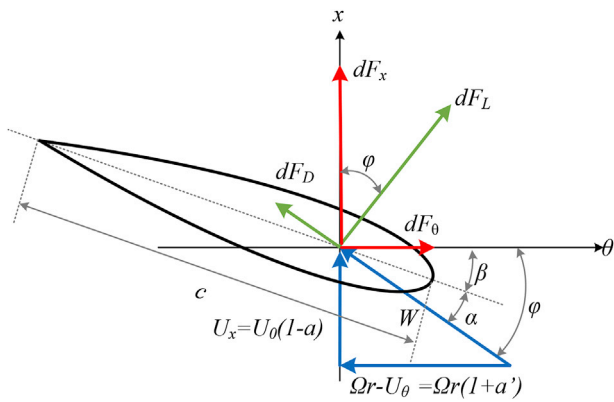


Fig. 3. Cross-sectional blade element showing velocity and forces.

(Bossanyi, 2003) are used for the 2.4 MW utility-scale turbine, and the corresponding Reynolds number is 2×10^6 . On the other hand, the Reynolds number for the airfoils of the model turbine in the wind tunnel test is around 5×10^4 . Therefore, the lift force coefficients are modified based on the NACA0012 provided by Burton et al. (2011) to reproduce the low Reynolds number effect. The drag force coefficients of the blade are not sensitive to the Reynolds number so the data for the sample 2 MW offshore wind turbine are used. The aerodynamic force coefficients for each section of the blade are plotted for low (5×10^4) and high Reynolds

number (2×10^6) in Fig. 4, in which the ‘tr’ denotes the blade thickness ratio.

The thrust coefficients of whole rotor are calculated under different tip speed ratios as shown in Fig. 5 to validate the accuracy of the adopted aerodynamics coefficients for the blades. It can be seen that the predicted thrust coefficients show good agreement with the measured data from the wind tunnel and field test for the model and utility scale wind turbine, respectively. The predicted tangential force is compared with the measured one from the field test for the utility scale wind turbine as shown in the reference (Yousefi et al., 2016).

The load distributions on the blade under different thrust coefficients are presented in Fig. 6, in which the forces on the rotor disk calculated by Eq. (12) and Eq. (13) are multiplied by the rotor width and normalized by $1/2\rho U_h^2$. It can be seen that when the rotor thrust coefficient has similar values, the distribution of the resulting axial and tangential forces along the rotor is analogous. The behavior of the wake is insensitive for the Reynolds number of a blade as mentioned by Whale et al. (Whale et al., 2000). The small difference on the load distribution does not cause distinct effects on the wake flow. This implies that effects of Reynolds number and blade details are not obvious on the wake flows of wind turbines as shown in section 2.5.

In the present wind turbine model, the nacelle and tower are modelled as porous media with 99.9% packing density. The forces induced by the nacelle and tower are calculated as follows:

$$f_{n,i} = -\frac{1}{2} \rho C_{D,i} |u_i| u_i \tag{18}$$

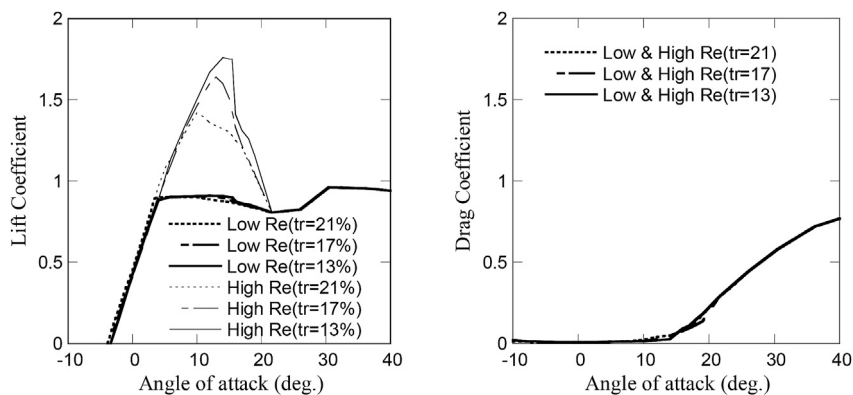


Fig. 4. Variation of airfoil aerodynamic coefficients with the attack angle: (a) Lift and (b) Drag force coefficients.

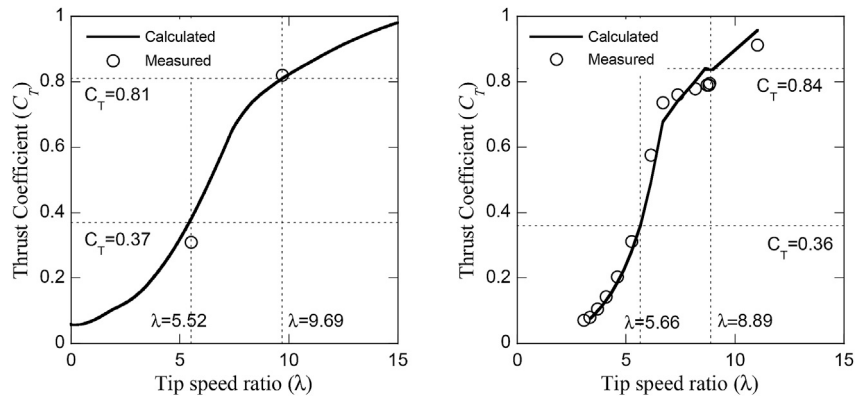


Fig. 5. Variation of the thrust coefficient with tip speed ratio of (a) model wind turbine and (b) utility-scale wind turbine.

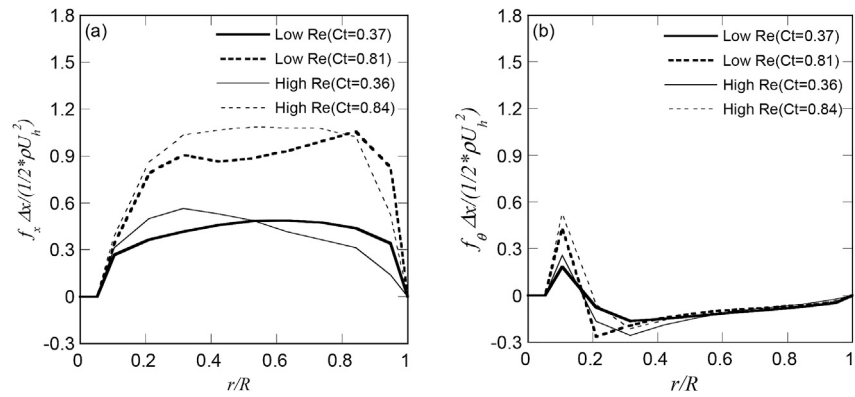


Fig. 6. Radial distribution of rotor load calculated by BEM theory: (a) axial direction, (b) tangential direction.

where u_i is the local velocity inside the nacelle and tower and should be close to 0. Thus, the drag coefficient $C_{D,i}$ is set to 1×10^5 in the CFD simulation.

2.3. Numerical setup

Numerical simulations are conducted in the atmospheric boundary layer simulated by using the same spires and fence as the wind tunnel test by Ishihara et al. (2004). As shown in Fig. 7(a), the computational domain has a streamwise length of 18.5 m, a spanwise length of 1.5 m and a vertical height of 1.8 m. The wind turbine model shown in Fig. 7(b)

is placed at a distance of 5.5 m from the fence and at the center in the spanwise direction. The rotor diameter D is 0.57 m and the hub height H is 0.7 m. The velocity-inlet boundary condition is used with a uniform velocity of 10 m/s (same as the wind tunnel test) and the outlet is set as outflow (zero gradient of velocity). Symmetry boundary conditions are imposed at the top and side boundaries. The no-slip wall boundary condition is used for the bottom of the wind tunnel and the surface of spires and fence. The rotor disk, nacelle and tower as shown in Fig. 7(b) are divided in a uniform distance of 0.01 m by tetrahedral mesh. The low turbulence flow is generated by using the spires as shown in Fig. 8(a) and the high turbulence flow is generated by using the combination of wider

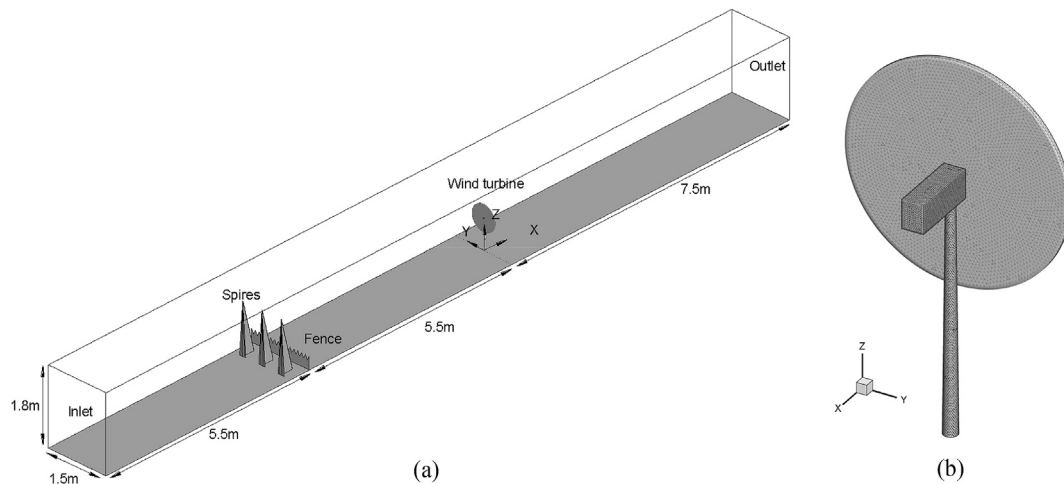


Fig. 7. Schematic of (a) the computational domain and (b) wind turbine model.

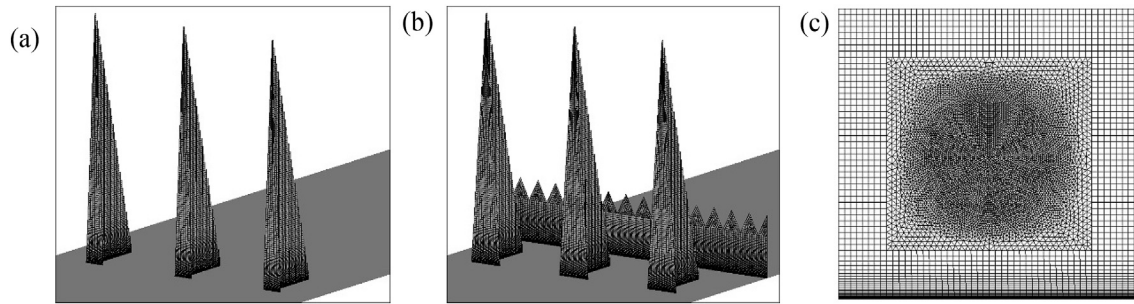


Fig. 8. Grid used in the numerical simulation: (a) spires for the low turbulence inflow, (b) spires and fence for the high turbulence inflow, (c) the rotor section.

spires and fence as shown in Fig. 8(b). The minimum grid size for the spires and fence in vertical and horizontal direction are set to 0.01 m and 0.002 m, respectively. The turbine rotor is connected smoothly with the outside domain as shown in Fig. 8(c), where the front surface of the rotor is located at $x = 0$.

It should be noted that the wake simulations for utility-scale turbine are also done in the wind tunnel scale since the wake flow behavior itself is insensitive to the Reynolds number when it is larger than 1×10^3 (Sørensen et al., 1998). In the actuator disc simulation, the Reynolds number effects from the blade aerodynamics are taken into account by the drag and lift coefficients as shown in Fig. 4.

Two kinds of operating condition ($C_T \approx 0.35$ and $C_T \approx 0.8$) under two types of inflow with different ambient turbulence intensity ($I_a = 0.035$ and $I_a = 0.137$) are used for the model and utility-scale wind turbines, respectively. For the model wind turbine, the tip speed ratio is set the same as the wind tunnel test. The parameters of numerical simulation for each case are summarized in Table 1, in which I_a is the ambient turbulence intensity at the hub height, C_T is the thrust coefficient and is defined as:

$$C_T = \frac{T}{0.5\rho U_h^2 A_D} \tag{19}$$

where A_D is the area of the rotor disk, T is the thrust force acting on the rotor and U_h is the hub height mean velocity. WT-M and WT-P denote the turbine model used in the wind tunnel test and the utility-scale turbine used at the Choshi demonstration site, respectively.

2.4. Inflow

The atmosphere boundary layers without wind turbine are generated by the spire and fence as the wind tunnel test. The mean velocities at the hub height with the low and high turbulence intensity are 10.22 m/s and 10.24 m/s, respectively, which are close to each other. All profiles of the mean velocity in this study are normalized by $U_h = 10.2$ m/s. The turbulence intensity is defined as:

$$I_1 = \frac{\sigma_u}{U_h} \tag{20}$$

Table 1
Parameters of numerical simulation.

Case	WT-Type	C_T	I_a	Re	Tip speed ratio λ	Pitch Angle (deg.)
1	WT-M	0.37	0.035	5×10^4	5.52	0
2	WT-M	0.81	0.035	5×10^4	9.69	0
3	WT-M	0.37	0.137	5×10^4	5.52	0
4	WT-M	0.81	0.137	5×10^4	9.69	0
5	WT-P	0.36	0.035	2×10^6	5.66	7.4
6	WT-P	0.84	0.035	2×10^6	8.89	0
7	WT-P	0.36	0.137	2×10^6	5.66	7.4
8	WT-P	0.84	0.137	2×10^6	8.89	0

where σ_u is turbulence standard deviation. The ambient turbulence intensities at the hub height are $I_a = 0.035$ and $I_a = 0.0137$ for low and high turbulence conditions, respectively. As shown in Fig. 9, the vertical mean velocity and turbulence intensity profiles at the location of the turbine ($x = 0, y = 0$) show good agreement with the experiment data. The significant gradient for the turbulence intensity as shown in Fig. 9 (b) is due to the inflow profile generated by the fence and spires and the fully developed ABL profile is observed before the model wind turbine.

2.5. Mean velocity and turbulence intensity

The characteristics of mean velocity and turbulence intensity in the wake region are shown in Figs. 10 and 11. The two-dimensional contours from the model turbine cases (WT-M) are displayed in the vertical x - z plane through the center of the turbine ($y = 0$) as well as in the horizontal x - y plane at the hub height ($z = H$). The predicted vertical and horizontal profiles at selected downwind locations of $x = 2D, 4D, 6D$ and $8D$ are also plotted to illustrate the quantitative comparison between simulation results and the experiment data. Black solid lines and dash lines denote the results for the model wind turbine (WT-M) and the utility-scale wind turbine (WT-P), respectively. The experiment data are shown by open circles at two positions of $x = 2D, 8D$. All velocities are normalized by the hub height mean velocity U_h . The x -axis denotes the distance from the wind turbine normalized by the rotor diameter D . The distance of $2D$ corresponds to a unit scale of normalized mean velocity U/U_h in Fig. 10 and a scale of turbulence intensity with the value of 0.3 in Fig. 11, respectively.

As shown in Fig. 10(a)–(d), mean velocities in the wake region show significant differences with different ambient turbulence intensity and thrust coefficients. It can be seen that high ambient turbulence intensity (Case 1, 2, 5, 6) leads to shorter wake region than cases with the low ambient turbulence (Case 3, 4, 7, 8). The high turbulence accelerates the process of flow mixing in the wake region. In addition, the large thrust coefficient cases (Case 2, 4, 6, 8) induces stronger velocity deficit in the wake region than the cases with small thrust coefficient (Case 1, 3, 5, 7).

In Fig. 10(e)–(h), the horizontal profiles show axial symmetric and some asymmetry in near wake region is due to the effect of torque on the rotor.

The LES simulation results of both model and utility-scale wind turbine trend towards the experimental data, even though the velocity deficits are slightly underestimated in the near wake region ($x = 2D$) for the low turbulence cases (Case1, 2, 5 and 6). As mentioned in the references (Vermeer et al., 2003; Xie and Archer, 2014), the near wake flow is significantly affected by the specific blade aerodynamics when the ambient turbulence is very low, because the ADM-R model is difficult to consider all detailed information for the blades. However, these differences are negligible in the engineering applications with a real ambient turbulence intensity. For the high ambient turbulence cases (Case 3, 4, 7 and 8), the velocity deficits in the near wake region are well predicted, since larger ambient turbulence generates stronger flow mixing and makes the effect from the blades less obvious.

Fig. 11(a)–(d) reveal that an obvious enhancement of turbulence

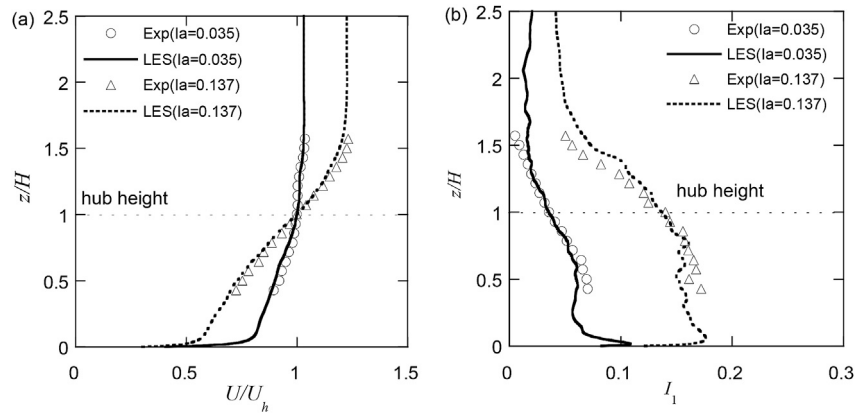


Fig. 9. Inflow profiles: (a) Mean velocity; (b) Turbulence intensity.

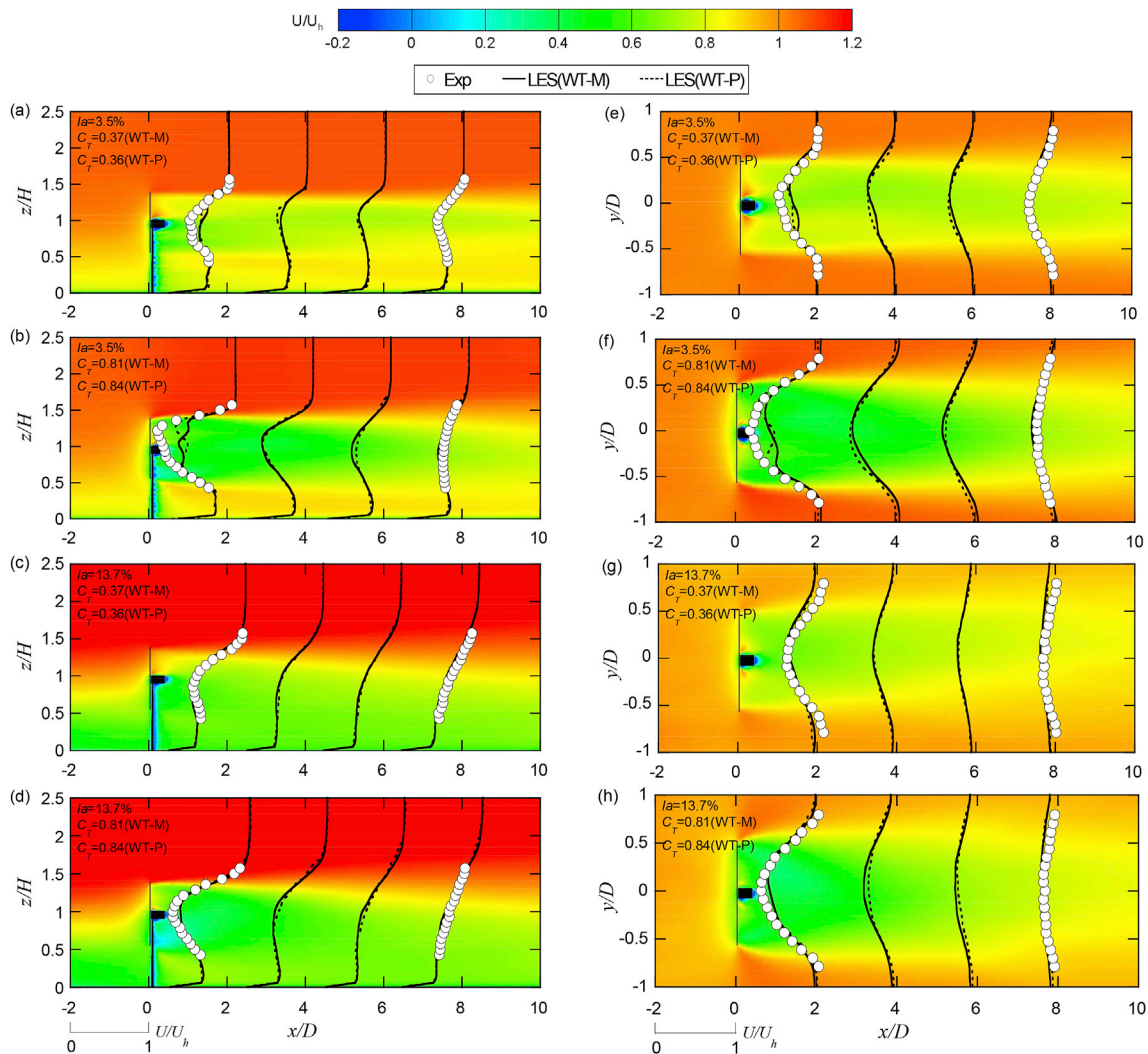


Fig. 10. Mean velocity profiles and contours: (a) Case 1 and 5, (b) Case 2 and 6, (c) Case 3 and 7, (d) Case 4 and 8 in the vertical x - z plane through the center of the rotor; (e) Case 1 and 5, (f) Case 2 and 6, (g) Case 3 and 7, (h) Case 4 and 8 in the horizontal x - y plane at the hub height.

occurs in the upper half of the wake region, especially at the top tip height. This enhancement is related to the wind shear that is the sharp shape of mean velocity profile near the top tip as shown in Fig. 10. In the lower part of the wake flow, the added turbulence intensity is weakened. It is due to the strong turbulence mixing near the ground. It can also be

seen that larger thrust coefficient cases exhibit larger turbulence intensity in the wake flow and the maximum turbulence intensity occurs in the near wake region (about $2D$ downwind). Meanwhile, it can be clearly observed that the nacelle and tower also generate considerable turbulence but it vanishes quickly in the near wake region.

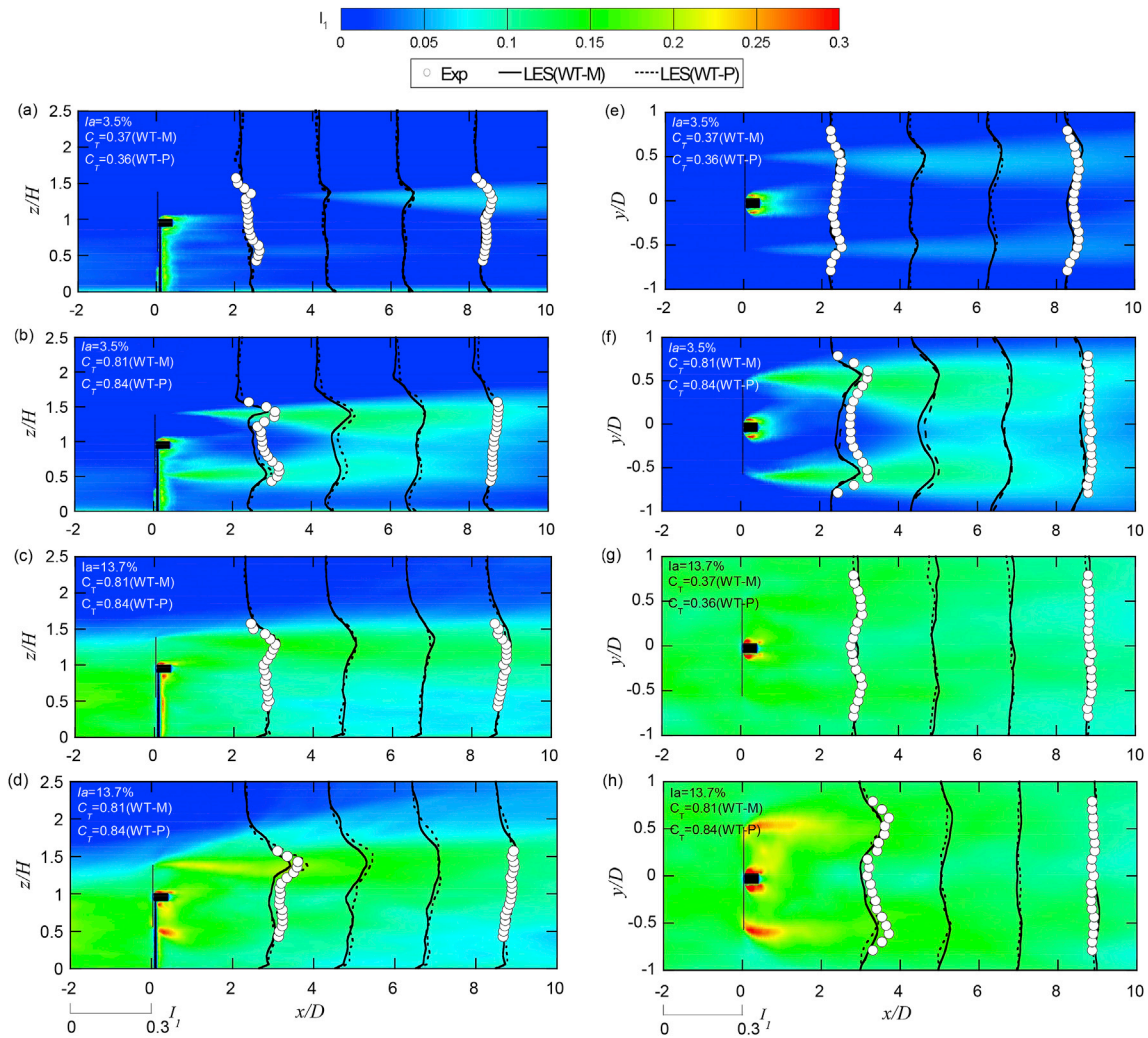


Fig. 11. Turbulence intensity profiles and contours: (a) Case 1 and 5, (b) Case 2 and 6, (c) Case 3 and 7, (d) Case 4 and 8 in the vertical x - z plane through the center of the rotor; (e) Case 1 and 5, (f) Case 2 and 6, (g) Case 3 and 7, (h) Case 4 and 8 in the horizontal x - y plane at the hub height.

The turbulence intensities in the horizontal x - y plane at the hub height present a dual-peak and approximately axisymmetric distribution with the maximum value near the two side-tip position as shown in Fig. 11(e) ~ (h). They are related to the strong shear layer in the wake boundary region. Both horizontal contours and profiles display a slight asymmetry due to the effect of torque on the rotor.

Generally, the LES simulation results of mean velocity and turbulence intensity in the wake flow show good agreement with the experiment data for the model wind turbine. The emphasis is that the mean velocity and turbulence intensity in the wake region of model and utility-scale wind turbines show quite close profiles for each case. It implies that the wake flow strongly depends on the thrust coefficient C_T and ambient turbulence intensity I_a , but weakly depends on the Reynolds number and the specific blade type.

3. A new wake model

A new wake model is proposed for prediction of velocity deficit and added turbulence intensity and derived in section 3.1 and 3.2. The predicted values by the proposed and conventional models are compared with those obtained from the LES simulations and wind tunnel tests. The applicability of the wake model used in IEC61400-1 and the proposed model for the local turbulence intensity prediction in the wake region are investigated and compared with LES results in section 3.3.

3.1. Velocity deficit

The fully developed wake flow behind still bluff bodies like cylinder and disk have been investigated (Schlichting, 1979; Johansson et al., 2003). The assumption of axisymmetric and the self-similar distribution for the velocity deficit in the far wake region were used in these studies.

In this study, the streamwise velocity deficit induced by the rotor is also assumed to be axisymmetric with respect to the axis of the rotor and have self-similar distribution in the wake cross-section. Therefore, the mean velocity $U(x, y, z)$ in the wake can be determined by the following equation:

$$U(x, y, z) = U_0(y, z) - \Delta U \tag{21}$$

where $U_0(y, z)$ is the wind speed of incoming flow and ΔU is the velocity deficit induced by the turbine rotor and is a function of x and r which denotes the radial distance from the center of the wake as $r = \sqrt{y^2 + (z - H)^2}$. Since the velocity deficit shows self-similar property, it can be expressed as the product of a streamwise function and a self-similar shape function:

$$\Delta U / U_h = F(C_T, I_a, x/D) \phi(r/\sigma) \tag{22}$$

where $F(C_T, I_a, x/D)$ represents the maximum velocity deficit ΔU_{\max} for

each downwind location normalized by the mean wind speed U_h at the hub height, $\phi(r/\sigma)$ is the self-similar distribution of the velocity deficit on the cross section, which is defined as the velocity deficit normalized by the maximum value at the center of the wake section. σ denotes the standard deviation of the mean velocity deficit distribution in the spanwise direction at each cross section and is treated as the representative wake width. $F(C_T, I_a, x/D)$ and $\phi(r/\sigma)$ are termed as “streamwise function” and “spanwise function” for the velocity deficit in this study, respectively.

The Gaussian distribution assumption has been derived by Ishihara et al. (2004) (see Appendix A) and is used as the spanwise function for the velocity deficit in this study as follows:

$$\phi(r/\sigma) = \exp\left(-\frac{r^2}{2\sigma^2}\right) \quad (23)$$

Fig. 12(a) shows the schematic of the Gaussian distribution for velocity deficit. The velocity deficit profiles of selected positions in the horizontal plane at the hub height are normalized by the maximum value ΔU_{\max} and plotted in Fig. 12(b). The distance from the rotor center is normalized by the wake half-width $r_{1/2}$, which is widely used as the characteristic wake width (Bastankhah and Porté-Agel, 2014). $r_{1/2}$ is defined as the half the spanwise distance between two points on a profile at which the mean deficit is half of its maximum. For the Gaussian distribution, it has an expression as $r_{1/2} = \sqrt{2\ln 2}\sigma$, σ can be determined by $r_{1/2}$ for each spanwise profile as shown in Fig. 12(b). The Gaussian distribution against $r/r_{1/2}$ is also plotted by solid line for comparison. As expected, the LES data generally show good agreement with the Gaussian distribution in spite of the slight asymmetry in the near wake region.

Similar to Bastankhah and Porté-Agel (Bastankhah and Porté-Agel, 2014), the current study also assumes linear expansion of the wake region downstream of the turbine and σ/D is defined as:

$$\frac{\sigma}{D} = k^* \frac{x}{D} + \varepsilon \quad (24)$$

By taking the Gaussian distribution and the self-similarity assumption, Bastankhah and Porté-Agel (Bastankhah and Porté-Agel, 2014) derived a streamwise function. However, this analytical solution may diverge in the near wake region as discussed in Appendix B. Therefore, the first order approximation of Taylor expansion for Eq. (B.8) is made to find an expression for the far wake region as shown in the following equation:

$$C(x) = \frac{C_T}{16(k^*x/D + \varepsilon)^2} \quad (25)$$

Eq. (25) is rewritten in a general form as follows:

$$F(C_T, I_a, x/D) = \frac{1}{(a + b \cdot x/D)^2} \quad (26)$$

where a and b are the model parameters which can be derived by

equating Eq. (26) with Eq. (25) as follows:

$$a = 4C_T^{-0.5}\varepsilon, \quad b = 4C_T^{-0.5}k^* \quad (27)$$

A specific expression for k^* has not been given in the reference (Bastankhah and Porté-Agel, 2014). In this study, k^* and ε in Eq. (24) are modelled as a function of C_T and I_a . In order to obtain constants in the parameters, except for the results of 8 cases conducted in this study, data from another 9 cases in references (Wu and Porté-Agel, 2012) and (Wu and Porté-Agel, 2011) are also used. There are 10 data points for C_T (0.36, 0.37, 0.81, 0.84, 0.8, 0.461, 0.375, 0.45, 0.55, 0.476) and 7 data points for I_a (0.035, 0.137, 0.048, 0.069, 0.094, 0.134, 0.07) to fit constants in the parameters. Finally, the empirical expression for k^* and ε are proposed by data fitting in the far wake region based on Eq. (25).

$$k^* = 0.11C_T^{1.07}I_a^{0.20}, \quad \varepsilon = 0.23C_T^{-0.25}I_a^{0.17} \quad (28)$$

Inserting Eq. (28) into Eq. (27), the parameters a and b are determined as:

$$a = 0.93C_T^{-0.75}I_a^{0.17}, \quad b = 0.42C_T^{0.6}I_a^{0.2} \quad (29)$$

It should be noted that Eq. (26) can only be used for the far wake region and a correction term p should be added to modify the streamwise function in the near wake region as follows:

$$F(C_T, I_a, x/D) = \frac{1}{(a + b \cdot x/D + p)^2} \quad (30)$$

The correction term p in the near wake region should decrease with the distance downwind turbine and can be modelled by a similar form as Eq. (26), i.e. $p \propto (1 + x/D)^{-2}$. As mentioned in section 2, the influence from turbine aerodynamics is weakened by the high ambient turbulence and large thrust coefficient, thus the correction term can be written as $p \propto C_T^{-\alpha}I_a^{-\beta}(1 + x/D)^{-2}$. The model parameters α and β are obtained by data fitting and expressed as shown in the following equation:

$$p = 0.15C_T^{-0.25}I_a^{-0.7}(1 + x/D)^{-2} \quad (31)$$

The final form of the proposed model and parameters for the velocity deficit are summarized in the Table 2. The new model is general applicable in both near and wake region.

Fig. 13 shows the variation of normalized velocity deficit at the hub height with normalized distance downwind the turbine. The experimental data are marked by the triangles and the LES results denoted by the open circles and crosses are the value measured along the line in the streamwise direction through the rotor center. The solid lines denote the result of the proposed model and dotted lines are the result from the model by Katic et al. (1986), which is expressed as follows:

$$\frac{\Delta U}{U_h} = \frac{1 - \sqrt{1 - C_T}}{(1 + 2kx/D)^2} \quad (32)$$

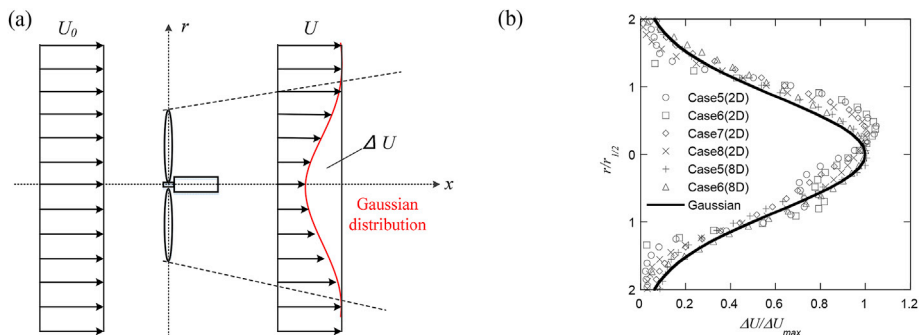


Fig. 12. Gaussian distribution for velocity deficit: (a) Schematic and (b) Numerical simulations.

Table 2
Summary of the new wake model.

Wake model	Formulas	Parameters
Representative wake width	$\sigma/D = k^* x/D + \varepsilon$	$k^* = 0.11C_T^{1.07}I_a^{0.20}$ $\varepsilon = 0.23C_T^{0.25}f_a^{0.17}$
Velocity deficit	$\Delta U(x,y,z)/U_h = \frac{1}{[a+b-x/D+c(1+x/D)^2]^2} \exp\left(-\frac{r^2}{2\sigma^2}\right), \quad r = \sqrt{y^2 + (z-H)^2}$	$a = 0.93C_T^{-0.75}f_a^{0.17}$ $b = 0.42C_T^{0.6}I_a^{0.2}$ $c = 0.15C_T^{0.25}I_a^{-0.7}$
Added turbulence intensity	$\Delta I_1(x,y,z) = \frac{1}{d+e-x/D+f(1+x/D)^2} \left\{ k_1 \exp\left(-\frac{(r-D/2)^2}{2\sigma^2}\right) + k_2 \exp\left(-\frac{(r+D/2)^2}{2\sigma^2}\right) \right\} - \delta(z),$ $\delta(z) = \begin{cases} 0 & (z \geq H) \\ I_a \sin^2\left(\pi \frac{H-z}{H}\right) & (z < H) \end{cases}$	$d = 2.3C_T^{-1.2}$ $e = 1.0f_a^{0.1}$ $f = 0.7C_T^{-3.2}I_a^{-0.45}$ $k_1 = \begin{cases} \cos^2(\pi/2 \cdot (r/D - 0.5)) & r/D \leq 0.5 \\ 1 & r/D > 0.5 \end{cases}$ $k_2 = \begin{cases} \cos^2(\pi/2 \cdot (r/D + 0.5)) & r/D \leq 0.5 \\ 0 & r/D > 0.5 \end{cases}$

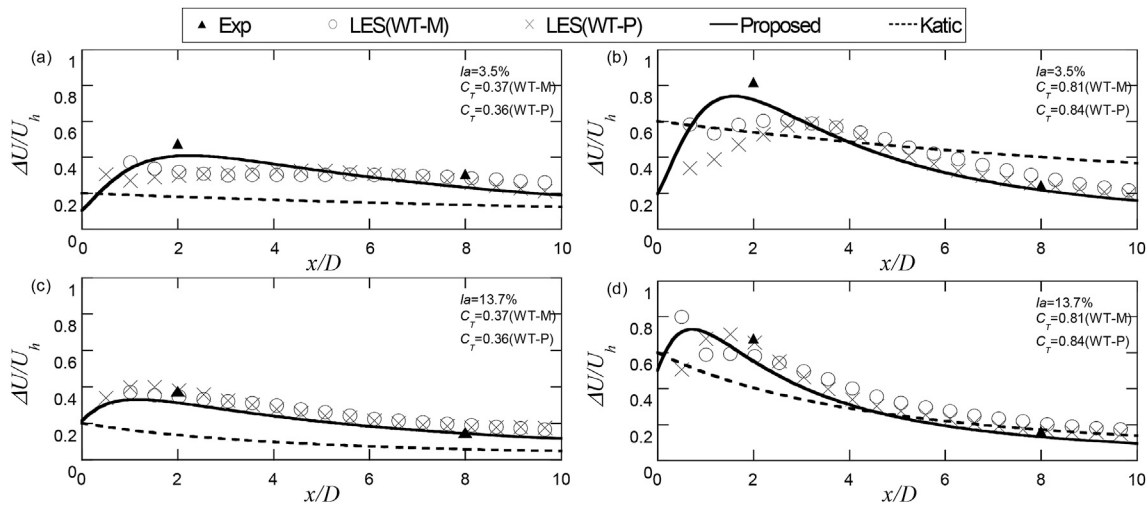


Fig. 13. Variation of normalized velocity deficit at the hub height with normalized distance downwind the turbine: (a) Case 1 and 5, (b) Case 2 and 6, (c) Case 3 and 7, (d) Case 4 and 8.

where k is the wake decay coefficient and the recommend values is $k = 0.4I_a$ for the flat terrain under neutral conditions (Peña et al., 2016).

As can be seen from Fig. 13, the proposed model shows good agreement with the LES data for all case in the near as well as the far wake region. The model by Katic et al. generally underestimates the velocity deficit since it uses the top-hat shape. The velocity deficits reach maximum in the near wake region and decrease more slowly for the low ambient turbulence cases than those for the high ambient turbulence cases. The predicted velocity deficits by the proposed model catch these behaviours well.

The validation metric, hit rate q (Schatzmann et al., 2010) is used here to quantify the agreement between LES results and values predicted by wake models. q is defined as:

$$q = \frac{1}{N} \sum_{i=1}^N n_i, \quad n_i = \begin{cases} 1 & \left| \frac{y_i - x_i}{x_i} \right| \leq D_q \text{ or } |y_i - x_i| \leq W_q \\ 0 & \text{else} \end{cases} \quad (33)$$

where, y_i and x_i are the observed (LES) and predicted (wake model) values of a given variable for sample i , respectively, and N is the number of data points. A hit rate q specifies the fraction of model results that differ within an allowed range D or W from the comparison data. D accounts for the relative uncertainty of the predicted values, and W describes the repeatability of the predicted values. The ideal values of the metrics that correspond to perfect agreement is 1.0 for q . The thresholds

for q are $D_q = 0.15$ for mean wind speed and $D_q = 0.21$ for turbulence intensity since the standard deviation of variable gives error as $\sqrt{2}$ as the variable itself. $W_q = 0.05|max|$ is used for both mean wind speed and turbulence intensity, in which $|max|$ is a maximum value supposed in the observation.

Fig. 14 shows scatter plots for comparison between the wake model and the LES results for normalized velocity deficit at the hub height, together with the corresponding validation metric boundary. The LES data from this study as well as those reported by Wu and Porté-Agel (2012) are used. The proposed model shows better performance for velocity deficit prediction with a higher hit rate than the Katic model as shown Table 3.

Fig. 15 compares the vertical as well as horizontal profiles of velocity deficit for each case obtained from the present LES results and the two wake models. It can be seen that the proposed model gives more reasonable distributions than the top-hat shape used by Katic et al. which underestimates the velocity deficit in the center of wake and overestimates them in the outside regions.

3.2. Added turbulence intensity

As presented in section 2.5, the turbulence distribution in the wake region also shows symmetric in the horizontal direction, and the non-symmetric character of turbulence distribution in the vertical distribution is associated with the non-symmetric character of the incident flow.

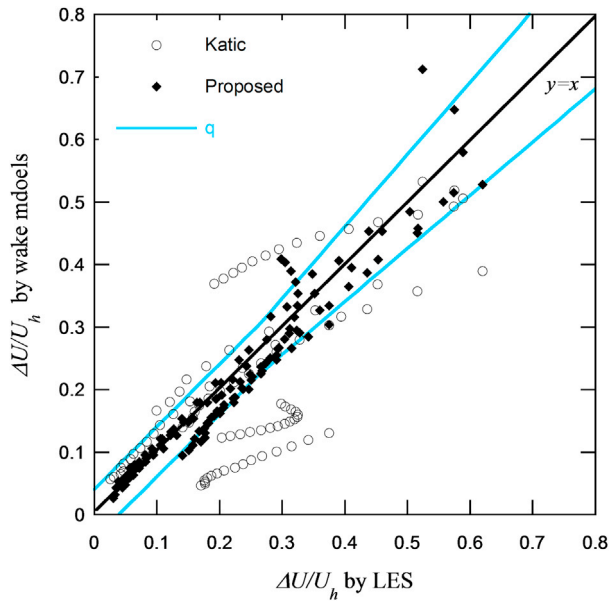


Fig. 14. Scatter plots for comparison between the wake model and the LES results for normalized velocity deficit at the hub height.

Table 3

Hit rate q for the wake models in the streamwise direction.

Wake model	$\Delta U/U_h$	ΔI_1
Proposed model	0.81	0.78
Katic	0.31	–
Crespo and Hernandez	–	0.38

Therefore, firstly the added turbulence intensity is assumed axial symmetric, and the effects of incoming shear layer are later considered to amend for the non-symmetry in the vertical direction. The turbulence standard deviation in any position $\sigma_u(x, y, z)$ downwind the turbine is determined by the ambient turbulence standard deviation $\sigma_{u_0}(y, z)$ and the added turbulence standard deviation $\Delta u'$ as shown in the following equation:

$$\sigma_u(x, y, z) = \sqrt{\sigma_{u_0}^2(y, z) + \Delta u'^2} \tag{34}$$

The self-similarity assumption is also taken for the added turbulence standard deviation $\Delta u'$ in this study for the first time, which is a function of x and r . The added turbulence intensity ΔI_1 can also be modelled as the product of the maximum value at the location x and the distribution function as follows:

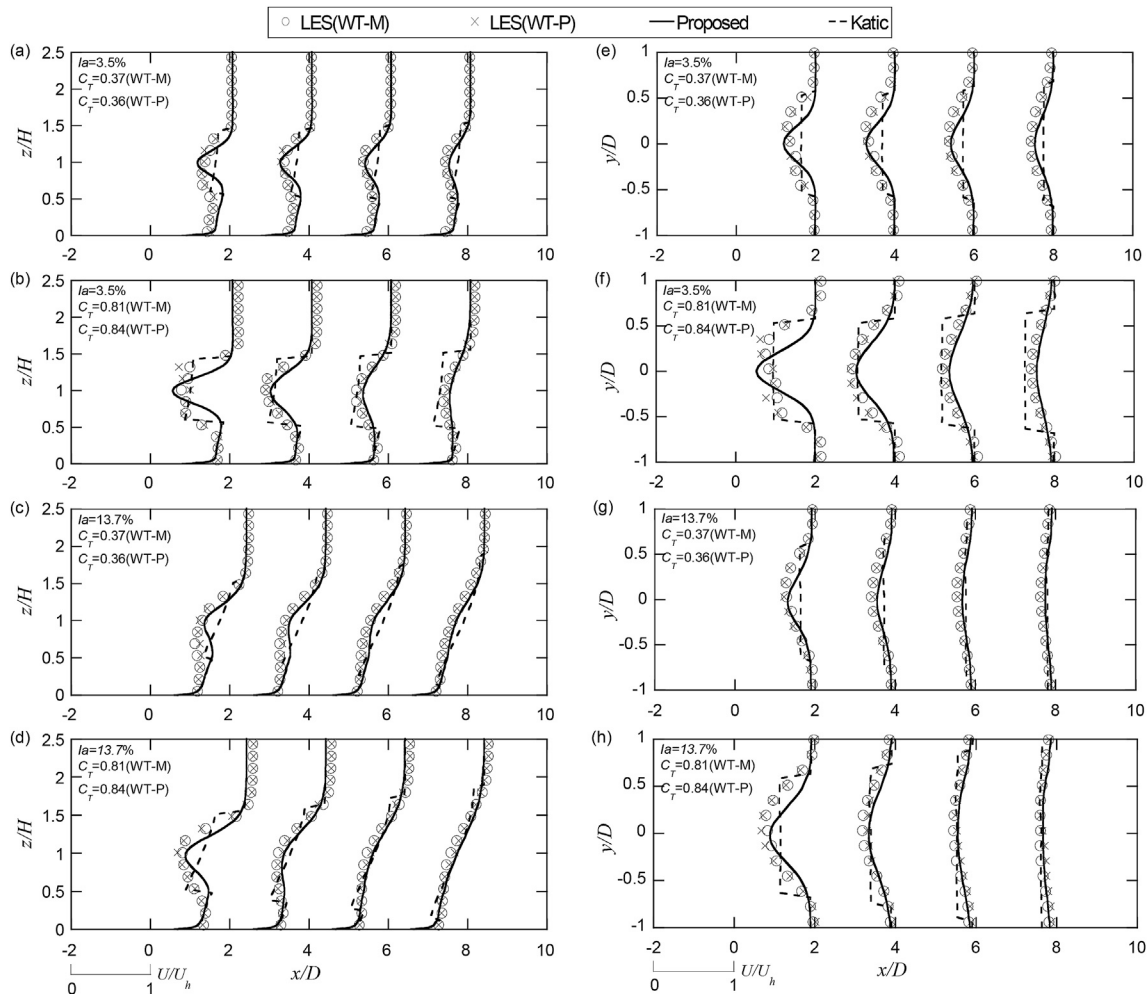


Fig. 15. Validation for mean velocity: (a) Case 1 and 5, (b) Case 2 and 6, (c) Case 3 and 7, (d) Case 4 and 8 for vertical direction, (e) Case 1 and 5, (f) Case 2 and 6, (g) Case 3 and 7, (h) Case 4 and 8 for horizontal direction.

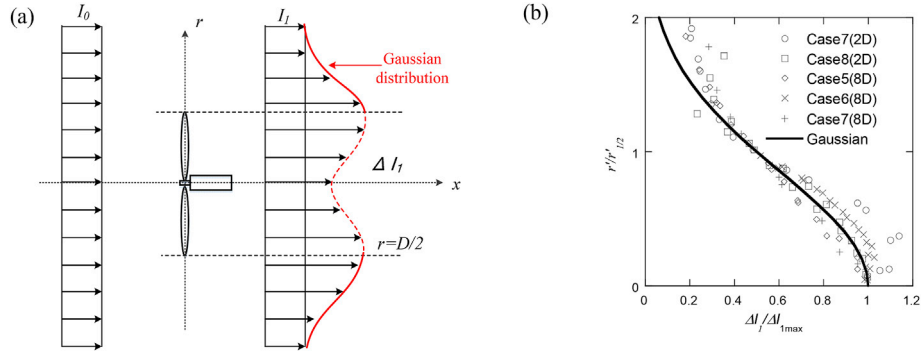


Fig. 16. Gaussian distribution for added turbulence intensity: (a) Schematic and (b) Numerical simulations.

$$\Delta I_1 = \frac{\Delta u'}{U_h} = G(C_T, I_a, x/D)\varphi(r/\sigma) \quad (35)$$

where $G(C_T, I_a, x/D)$ is the streamwise function denoting the maximum added turbulence intensity ΔI_{1max} at the tip of the blade for each downwind location, and $\varphi(r/\sigma)$ is the spanwise function which is assumed as a dual-Gaussian shape as shown in Fig. 16(a) and σ is the same parameter as in the Gaussian distribution for the velocity deficit.

The maximum value of added turbulence intensity occurs at the tip of blade instead of the center of the rotor. Similar to the velocity deficit distribution in the wake region, the Gaussian shape is used for the added turbulence intensity with peak of the distribution occurring at the rotor tip as shown in Fig. 16(a), and is expressed as:

$$\varphi(r/\sigma) = \exp\left(-\frac{r'^2}{2\sigma^2}\right) \quad (36)$$

In Fig. 16(b), the horizontal distributions of added turbulence intensity are plotted together with the Gaussian distribution, in which $r'_{1/2}$ is the half-width for added turbulence intensity distribution at one side. It can be seen that the added turbulence intensity can also be evaluated well by the Gaussian distribution. In Eq. (36), r' can be rewritten as $r' = r - D/2$. In the region between the tip sides ($r \leq D/2$) as shown in Fig. 16(a), the effect from each side can be combined by the superposition of the turbulence generated at the tip annulus. In this way, the distribution of added turbulence intensity in the spanwise direction can be expressed by the following equations:

$$\varphi(r/\sigma) = k_1 \exp\left(-\frac{(r - D/2)^2}{2\sigma^2}\right) + k_2 \exp\left(-\frac{(r + D/2)^2}{2\sigma^2}\right) \quad (37)$$

where k_1 and k_2 are the model parameters and are set to 1 and 0 in the outside region ($r > D/2$) and determined based on the continuity and monotonicity constraint when $r \leq D/2$ as shown in the following equations:

$$k_1 = \begin{cases} \cos^2(\pi/2 \cdot (r/D - 0.5)) & r/D \leq 0.5 \\ 1 & r/D > 0.5 \end{cases} \quad (38)$$

$$k_2 = \begin{cases} \cos^2(\pi/2 \cdot (r/D + 0.5)) & r/D \leq 0.5 \\ 0 & r/D > 0.5 \end{cases} \quad (39)$$

Assuming that the turbulence viscosity ν_t is constant and velocity deficit is small in the far wake region, namely $U(x, y, z) \approx U_0$, the transport equation of streamwise added turbulent standard deviation $\Delta u'^2$ has the same expression form as the transport equation of velocity deficit as shown in Eq. (A.3) (see Appendix A):

$$U_0 \frac{\partial(\Delta u'^2)}{\partial x} = \frac{\nu_t}{r'} \frac{\partial}{\partial r'} \left(r' \frac{\partial(\Delta u'^2)}{\partial r'} \right) \quad (40)$$

Therefore, similar to the expression of velocity deficit in Eq. (26), the maximum $\Delta u'^2$ for each downwind location in the wake region can be modelled analogically as:

$$\Delta u'^2_{max} = \frac{1}{(a' + b'x)^2} \quad (41)$$

The maximum added turbulence intensity ΔI_{1max} for each downwind location in the wake region can be expressed as:

$$\Delta I_{1max} = \frac{\Delta u'_{max}}{U_h} = G(C_T, I_a, x/D) = \frac{1}{d + e \cdot x/D} \quad (42)$$

where the parameter d and e are also a function of the thrust coefficient C_T and the ambient turbulence intensity I_a . Since the exponent of I_a for d and C_T for e are almost 0 by data fitting in the far wake region based on Eq. (42), d and e are expressed as follows:

$$d = 2.3C_T^{-1.2}, \quad e = 1.0I_a^{0.1} \quad (43)$$

As mentioned above for the velocity deficit modelling, it is also necessary to add a correction term q to consider the added turbulence intensity in the near wake region and the streamwise function is expressed by the following equation:

$$G(C_T, I_a, x/D) = \frac{1}{d + e \cdot x/D + q} \quad (44)$$

The correction term q in the near wake region is also obtained by the data fitting as shown in the following equation:

$$q = 0.7C_T^{-3.2}I_a^{0.45}(1 + x/D)^{-2} \quad (45)$$

Fig. 17 shows the variation of added turbulence intensity at the top tip height with the normalized distance downwind the turbine. The solid lines denote the results predicted by the proposed model and dotted lines are the results from the model by Crespo and Hernández (1996), which has the expression for the near and far wake regions as follows:

$$\Delta I_1 = \begin{cases} 0.362(1 - \sqrt{1 - C_T}) & (x < 3D) \\ 0.73 \left(\frac{1 - \sqrt{1 - C_T}}{2} \right)^{0.83} I_a^{-0.0325} \left(\frac{x}{D} \right)^{-0.32} & (x \geq 3D) \end{cases} \quad (46)$$

It can be seen that the proposed model captures the changing of ΔI_1 well for all the cases. In the far wake region, the Crespo and Hernández's model slightly underestimates ΔI_1 for small C_T cases and overestimates ΔI_1 for large C_T cases. On the other hand, it overestimates ΔI_1 in the near wake region for some cases.

Fig. 18 shows scatter plots for comparison between the wake model and the LES results for added turbulence intensity at the top-tip height, together with the corresponding validation metric boundary. The LES data from this study as well as those reported by Wu and Porté-Agel (2012) are used. The proposed model shows better performance for

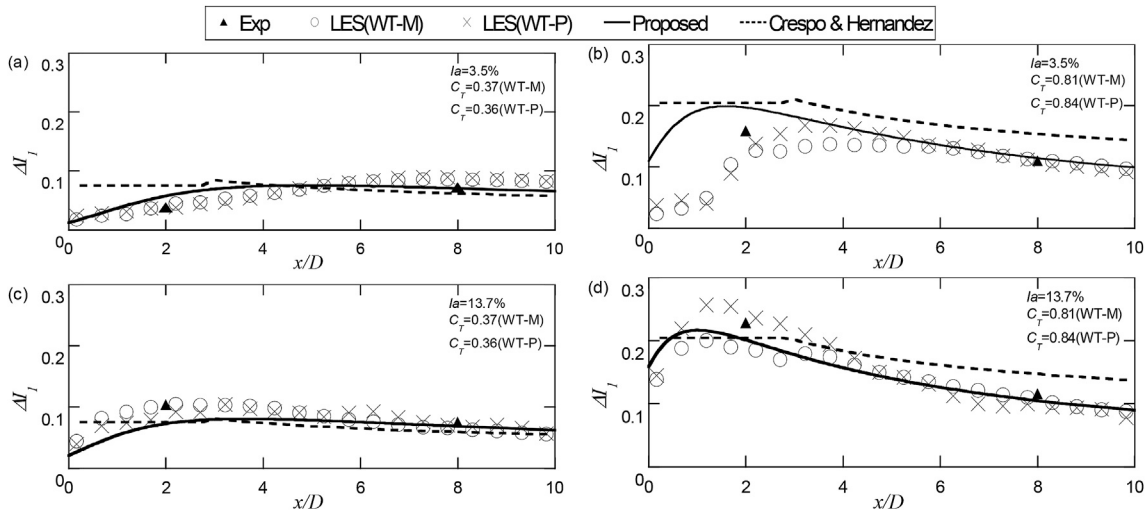


Fig. 17. Variation of added turbulence intensity at the top tip height with normalized distance downwind the turbine: (a) Case1 and 5, (b)Case2 and 6, (c)Case3 and 7, (d)Case4 and 8.

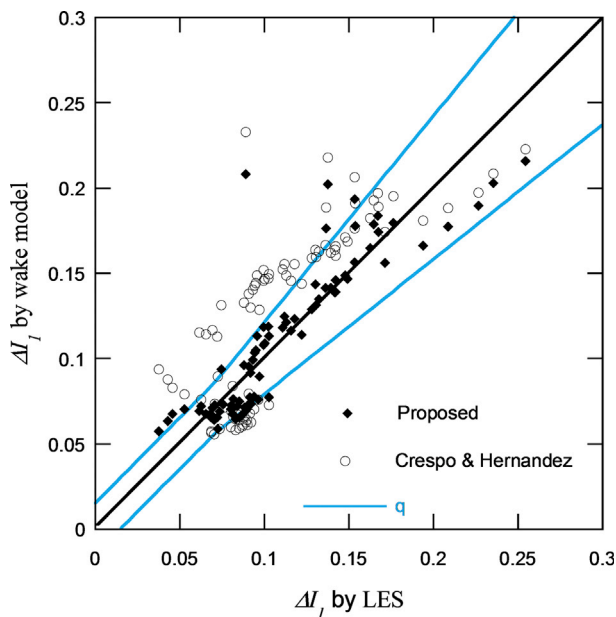


Fig. 18. Scatter plots for comparison between the wake model and the LES results for added turbulence intensity at the top-tip height.

added turbulence intensity prediction with a higher hit rate than the Crespo and Hernández's model as shown in Table 3.

In addition, a correction term $\delta(z)$ to describe the weakened turbulence intensity in the lower part of the wake flow is added as follows:

$$\delta(z) = \begin{cases} 0 & (z \geq H) \\ I_a \sin^2\left(\pi \frac{H-z}{H}\right) & (z < H) \end{cases} \quad (47)$$

The complete form of the proposed model for the added turbulence intensity is also summarized in Table 2.

Fig. 19 shows the vertical as well as horizontal profiles of turbulence intensity for each case obtained from the LES results and wake models. It can be clearly observed that the proposed wake model well predicts the spatial distributions and maximum values of the turbulence intensities, while the model based on the top-hat shape overestimates the turbulence intensity at the center of wake and underestimates them in the outside region.

3.3. Comparison with Frandsen's model

In the IEC61400-1 for wind turbine design (IEC 61400-1, 2005), the turbulence intensity in a wind turbine wake is estimated by the following formula:

$$\hat{\sigma}_T = \sqrt{\hat{\sigma}_w^2 + \hat{\sigma}_c^2} \quad (48)$$

where $\hat{\sigma}_T$ is the turbulence standard deviation in the wake region, $\hat{\sigma}_w$ is the turbulence standard deviation generated by the turbine and $\hat{\sigma}_c$ is the ambient turbulence standard deviation. The added turbulence intensity is defined as the $\hat{\sigma}_w$ normalized by the mean wind speed U_h at the hub height as follows:

$$\Delta I_1 = \frac{\hat{\sigma}_w}{U_h} = \frac{1}{1.5 + \frac{0.8}{\sqrt{C_T}} \frac{z}{D}} \quad (49)$$

This model by Frandsen (2007) was derived based on the data fitting at the wind speed in a range from 9 m/s to 11 m/s and the thrust coefficient C_T was about 0.7 based on the approximation of $C_T \approx 7/U_h$. In this model, the turbulence standard deviation is assumed to be constant in the cross section of the wake.

In addition, it should be noted that in the conventional wake models, including the proposed model, the added turbulence intensity is defined by reference of the mean velocity U_h at the hub height. However, the local turbulence intensity is crucial for a specific turbine load evaluation in the real wind farm as investigated by Göçmen and Giebel (2016). It is defined by the reference of local mean velocity and is expressed as follows:

$$\Delta I_1^{local} = \frac{\Delta I_1 \cdot U_h}{U} \quad (50)$$

where U is the local mean velocity in the wake region and is calculated based on Eq. (21).

In order to examine applicability of the proposed model and Frandsen's model, the local turbulence intensity predicted by the wake models and LES at hub height and top tip height are shown in Figs. 20 and 21. These two representative locations are chosen to consider that maximum mean velocity deficit at the hub height and the maximum added standard deviation at the top tip height, which might represent the maximum local turbulence intensity in the cross section of wake. The wind turbines are rarely laid close less than 2D, therefore the data in the wake region of $x/D > 2$ are shown. It can be seen that the local turbulence intensity

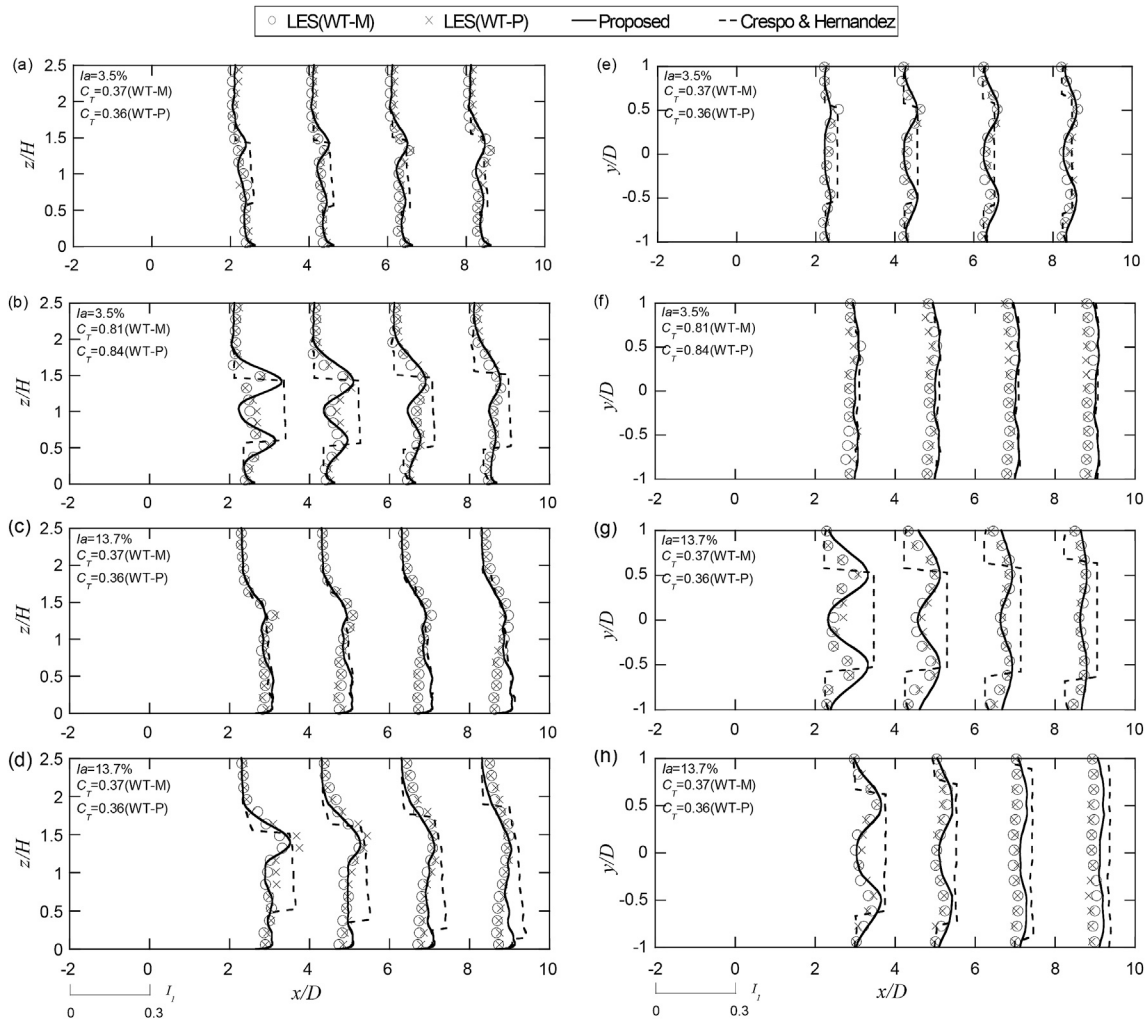


Fig. 19. Validation for turbulence intensity: (a) Case 1 and 5, (b) Case 2 and 6, (c) Case 3 and 7, (d) Case 4 and 8 for vertical direction, (e) Case 1 and 5, (f) Case 2 and 6, (g) Case 3 and 7, (h) Case 4 and 8 for horizontal direction.

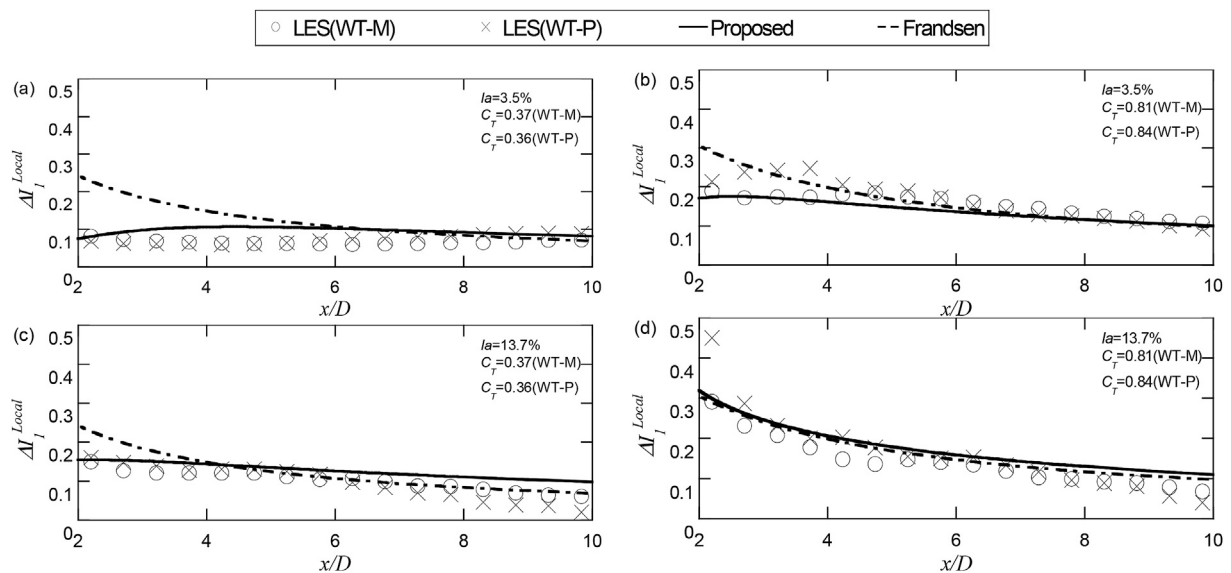


Fig. 20. Local added turbulence intensity at the hub height: (a) Case 1 and 5, (b) Case 2 and 6, (c) Case 3 and 7, (d) Case 4 and 8.

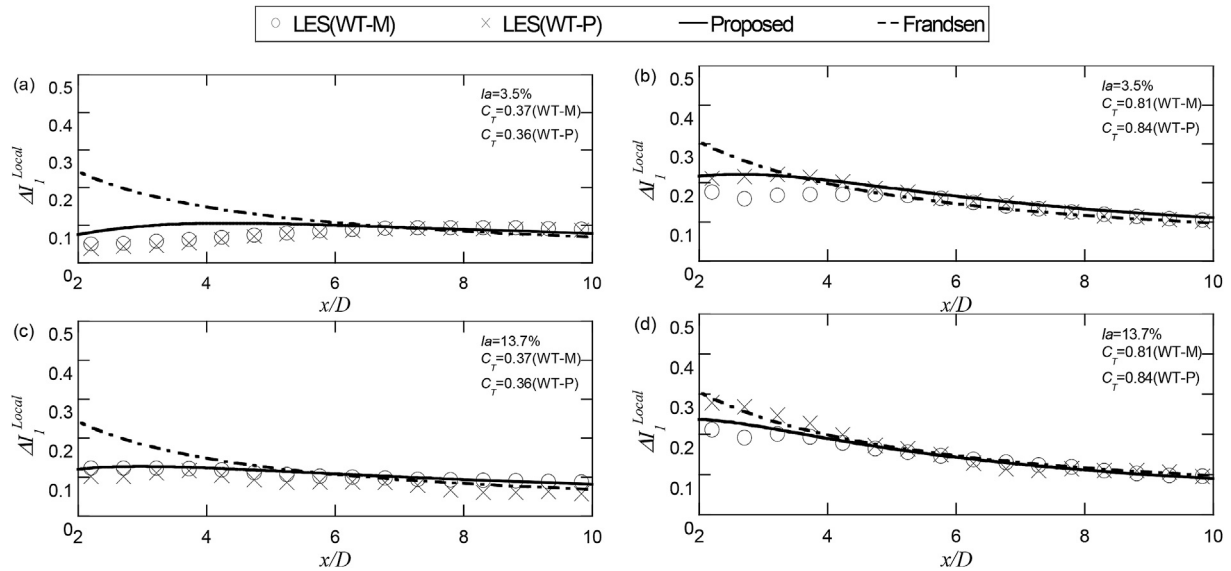


Fig. 21. Local added turbulence intensity at the top tip height: (a) Case1 and 5, (b) Case2 and 6, (c) Case3 and 7, (d) Case4 and 8.

predicted by the proposed model generally show good agreement with LES data in both near and far wake region. The Frandsen's model also shows good prediction in the far wake region but overestimates the values in the near wake region for small C_T cases since it is originally applicable to the case with $C_T \approx 0.7$ as mentioned above. It implies that the Frandsen's model is slightly conservative from the point of view of safety for the turbulence intensity prediction in near wake region under the condition with small thrust coefficient.

Similar to the approach implemented in reference (Niayifar and Porté-agel, 2016) for power prediction in a wind farm by using the single wake model of Bastanhah and Porté-Agel (2014), the proposed model can also be directly applied over a small-scale wind farm. On the other hand, inside a large-scale wind farm more with than 5 rows of wind turbine, the single wake model needs modifications as suggested in IEC standard (IEC 61400-1, 2005).

4. Conclusions

In this study, a series of numerical simulations of wind turbine wake with different ambient turbulence intensities and thrust coefficients are carried out by using LES for the model and utility-scale wind turbines. Subsequently, based on the numerical simulation result, a new wake model is proposed based on systematic analysis of the ambient turbulence intensity and the thrust coefficient effects on the wake flow. Following conclusions are obtained:

- (1) The numerical simulation results are in good agreement with the wind tunnel test. The mean velocity and turbulence intensity behind the model and utility-scale wind turbines show quite close profiles, which indicate that the thrust coefficient and ambient turbulence intensity are the dominant parameters for the wake flow in spite of the specific wind turbine type.
- (2) A new wake model is proposed to predict the mean velocity deficit and added turbulence intensity in the near and far wake region. The proposed model shows good performance for prediction of maximum values as well as distributions of mean velocity and turbulence intensity under various ambient turbulence and thrust coefficient conditions.
- (3) The applicability of the Frandsen's model used in IEC61400-1 and the proposed model for the local turbulence intensity prediction in the wake region are investigated. The proposed model provides more accurate predictions, while Frandsen's model shows conservative results in the near wake region.

Acknowledgements

This research was carried out as a part of the project funded by New Energy and Industrial Development Organization (NEDO) and Maeda Corporation. The authors wish to express their deepest gratitude to the concerned parties for their assistance during this study.

Appendix A. Gaussian distribution function in Ishihara's wake model

An axisymmetric wake allows a two-dimensional formulation in cylindrical coordinates. Here the distance from the center of rotor along axial and radial directions are denoted by x and r respectively, and the velocity in the wake region is described by:

$$U = U_0 - \Delta U \tag{A.1}$$

where U_0 is the wind speed of the incoming flow and ΔU denotes the velocity deficit.

When the wake flow is simplified without external forces and pressure gradients, the equation of momentum for steady axisymmetric wake flow can be expressed in cylindrical coordinates as follows:

$$U \frac{\partial U}{\partial x} + W \frac{\partial U}{\partial r} = \nu_r \left(\frac{\partial^2 U}{\partial x^2} + \frac{1}{r} \frac{\partial U}{\partial r} + \frac{\partial^2 U}{\partial r^2} \right) \tag{A.2}$$

where ν_t is the turbulence viscosity and is assumed to be constant. Since ΔU is small compared with U_0 , $W \frac{\partial \Delta U}{\partial r}$ and $\frac{\partial^2 \Delta U}{\partial x^2}$ is subsequently negligible. Eq. (A.2) can be simplified as Eq. (A.3) by inserting Eq. (A.1):

$$U_0 \frac{\partial \Delta U}{\partial x} = \frac{\nu_t}{r} \frac{\partial}{\partial r} \left(r \frac{\partial \Delta U}{\partial r} \right) \quad (\text{A.3})$$

The following equation can be obtained by applying the momentum conservation for the wake flow.

$$2\pi\rho U_0 \int (U_0 - U) r dr = \frac{1}{2} \rho U_0^2 C_T \pi \frac{D^2}{4} \quad (\text{A.4})$$

where C_T is the thrust coefficient of the turbine rotor and D is the diameter of rotor. Here, ΔU is neglected since it is smaller than U_0 .

In view of the similarity of the velocity profiles and the assumption of power law for the velocity deficit and wake width, the following expressions can be obtained as shown by Schlichting (1979):

$$\frac{\Delta U}{U_0} = Cx^p f(\eta), \quad \eta = \frac{r}{b} \quad (\text{A.5})$$

$$b = 2 \left(\frac{\nu_t}{U_0} \right)^{1+m} x^{-m} \quad (\text{A.6})$$

where C is a constant in the model of Ishihara et al. (2004) and η is the distance from the wake center r normalized by the representative wake width b which equals to $b_{1/2}/0.833$, C and ν_t are the function of the thrust coefficient as shown in the reference (Ishihara et al., 2004).

Substitution of Eqs. (A.5) and (A.6) into Eq. (A.3) yields

$$CU_0^2 (pf + m\eta f') x^{p-1} = \frac{1}{4} CU_0 \nu_t \left(\frac{U_0}{\nu_t} \right)^{2+2m} \left(\frac{1}{\eta} f' + f'' \right) x^{p+2m} \quad (\text{A.7})$$

in which the exponent of x at each side of the above equation should be equal, which leads to $m = -1/2$. Then by submitting it back to Eq. (A.7), the differential equation of η can be obtained as follows:

$$(\eta f')' + 2\eta^2 f' - 4p\eta f = 0 \quad (\text{A.8})$$

The boundary condition of the above equation are

$$\left. \begin{array}{l} f' = 0, f = 1 \quad (\eta = 0) \\ f = 0 \quad (\eta = \infty) \end{array} \right\} \quad (\text{A.9})$$

If p is set to -1 , the solution of the above differential equation is

$$f(\eta) = \exp(-\eta^2) \quad (\text{A.10})$$

Eq. (A.10) is an approximate solution of Eq. (A.8) and is used in this study.

Appendix B. Streamwise function in Bastanhah and Porté-Agel's wake model

If the viscous and pressure terms in the momentum equation are neglected, the following equation can be obtained for the wake by applying mass and momentum conservation:

$$2\pi\rho \int U(U_0 - U) r dr = \frac{1}{2} \rho U_0^2 C_T \pi \frac{D^2}{4} \quad (\text{B.1})$$

where U_0 is the wind speed of incoming flow, U is the wind speed in the wake region and C_T is the thrust coefficient of the turbine rotor. Eq. (B.1) is the same as Eq. (A.4) if ΔU^2 is neglected. The self-similarity in the wake describes the normalized velocity deficit as:

$$\frac{\Delta U}{U_0} = C(x) f(r/\delta) \quad (\text{B.2})$$

where $C(x)$, namely the streamwise function, represents the maximum normalized velocity deficit at each downwind location which occurs at the center of the wake, r is the radial distance from the wake center and δ is the characteristic wake width at each x . By taking the assumption of Gaussian distribution for the velocity deficit, Eq. (B.2) can be written as:

$$\frac{\Delta U}{U_0} = C(x) \exp\left(-\frac{r^2}{2\sigma^2}\right) \quad (\text{B.3})$$

Therefore, the wake velocity is given by:

$$U = U_0 \left(1 - C(x) \exp \left(-\frac{r^2}{2\sigma^2} \right) \right) \quad (\text{B.4})$$

Substituting for U from Eq. (B.4) into Eq. (B.1) and integrating from 0 to ∞ yields:

$$8 \left(\frac{\sigma}{D} \right)^2 C(x)^2 - 16 \left(\frac{\sigma}{D} \right)^2 C(x) + C_T = 0 \quad (\text{B.5})$$

By assuming σ/D as a constant, the above equation can be solved as follows:

$$C(x) = 1 - \sqrt{1 - \frac{C_T}{8(\sigma/D)^2}} \quad (\text{B.6})$$

In fact, σ/D slightly increases in the wake region and is written as:

$$\sigma/D = k^* x/D + \varepsilon \quad (\text{B.7})$$

Substituting it into Eq. (B.6),

$$C(x) = 1 - \sqrt{1 - \frac{C_T}{8(k^* x/D + \varepsilon)^2}} \quad (\text{B.8})$$

where k^* denotes the wake expansion rate and ε are expressed as follows,

$$\varepsilon = 0.2\sqrt{\beta} \quad \text{with} \quad \beta = \frac{1}{2} \frac{1 + \sqrt{1 - C_T}}{\sqrt{1 - C_T}} \quad (\text{B.9})$$

A specific expression for k^* has not been proposed by Bastankhah and Porté-Agel (2014), which consequently limits its applicability to other cases. In addition, it should be noted that the term in the square root, $1 - C_T/[8(k^* x/D + \varepsilon)^2]$, in Eq. (B.8) can be negative in the near wake region because Eq. (B.8) is an approximate solution of Eq. (B.5).

References

- Ainslie, J.F., 1988. Calculating the flowfield in the wake of wind turbines. *J. Wind Eng. Ind. Aerod.* 27, 213–224.
- Barthelmie, R.J., Hansen, K., Frandsen, S.T., Rathmann, O., Schepers, J.G., Schlez, W., Phillips, J., Rados, K., Zervos, A., Politis, E.S., Chaviaropoulos, P.K., 2009. Modelling and measuring flow and wind turbine wakes in large wind farms offshore. *Wind Energy* 12, 431–444.
- Bastankhah, M., Porté-Agel, F., 2014. A new analytical model for wind-turbine wakes. *Renew. Energy* 70, 116–123.
- Bossanyi, E.A., 2003. GH Bladed Version 3.51 User Manual.
- Burton, T., Sharpe, D., Jenkins, N., Bossanyi, E., 2011. *Wind Energy Handbook*, second ed. Wiley.
- Calaf, M., Meneveau, C., Meyers, J., 2010. Large eddy simulation study of fully developed wind-turbine array boundary layers. *Phys. Fluids* 22, 15110.
- Chamorro, L.P., Porté-Agel, F., 2009. A wind-tunnel investigation of wind-turbine wakes: boundary-layer turbulence effects. *Boundary-Layer Meteorol.* 132, 129–149.
- Crespo, A., Hernández, J., 1996. Turbulence characteristics in wind-turbine wakes. *J. Wind Eng. Ind. Aerod.* 61, 71–85.
- Crespo, A., Hernández, J., Frandsen, S., 1999. Survey of modelling methods for wind turbine wakes and wind farms. *Wind Energy* 2, 1–24.
- Ferziger, J.H., Perić, M. (Milovan), 2002. *Computational Methods for Fluid Dynamics*. Springer.
- Frandsen, S.T., 2007. Turbulence and Turbulence-generated Structural Loading in Wind Turbine Clusters. Risø National Laboratory for Sustainable Energy, Technical University of Denmark.
- Frandsen, S., Barthelmie, R., Pryor, S., Rathmann, O., Larsen, S., Hojstrup, J., 2006. Analytical modelling of wind speed deficit in large offshore wind farms. *Wind Energy* 9, 39–53.
- Gao, X., Yang, H., Lu, L., 2016. Optimization of wind turbine layout position in a wind farm using a newly-developed two-dimensional wake model. *Appl. Energy* 174, 192–200.
- Goit, J.P., Meyers, J., 2015. Optimal control of energy extraction in wind-farm boundary layers. *J. Fluid Mech.* 768, 5–50.
- Göçmen, T., Giebel, G., 2016. Estimation of turbulence intensity using rotor effective wind speed in Lillgrund and Horns Rev-I offshore wind farms. *Renew. Energy* 99, 524–532.
- Hassan, U., Glendinning, A.G., Morgan, C.A., 1990. A wind tunnel investigation of the wake structure and machine loads within small wind turbine farms. In: Proc. 12th BWEA Wind Energy Conference, pp. 47–52.
- IEC 61400-1, 2005. *Wind Turbines - Part 1: Design Requirements*.
- Ishihara, T., Yamaguchi, A., Fujino, Y., 2004. Development of a new wake model based on a wind tunnel experiment. In: *Glob. Wind Power*. <http://windeng.t.u-tokyo.ac.jp/ishihara/e/>.
- Jensen, N.O., 1983. A Note on Wind Generator Interaction. Risø National Laboratory for Sustainable Energy, Technical University of Denmark.
- Jiménez, Á., Crespo, A., Migoya, E., García, J., 2007. Advances in large-eddy simulation of a wind turbine wake. *J. Phys. Conf. Ser.* 75, 12041.
- Johansson, P.B.V., George, W.K., Gourlay, M.J., 2003. Equilibrium similarity, effects of initial conditions and local Reynolds number on the axisymmetric wake. *Phys. Fluids* 15, 603–617.
- Katic, I., Hojstrup, J., Jensen, N.O., 1986. A simple model for cluster efficiency. In: *European Wind Energy Conf. and Exhib.* 1986, pp. 407–410.
- Niayifar, A., Porté-Agel, F., 2016. Analytical Modeling of Wind Farms: a new approach for power prediction. *Energies* 9, 741.
- Oka, S., Ishihara, T., 2009. Numerical study of aerodynamic characteristics of a square prism in a uniform flow. *J. Wind Eng. Ind. Aerod.* 97, 548–559.
- Peña, A., Réthoré, P.-E., van der Laan, M.P., 2016. On the application of the Jensen wake model using a turbulence-dependent wake decay coefficient: the Sexbierum case. *Wind Energy* 19, 763–776.
- Quarton, D.C., Ainslie, J.F., 1989. Turbulence in wind turbine wakes. In: Proc. of the European Wind Energy Conference. BWEA/EWEA.
- Sanderse, B., van der Pijl, S.P., Koren, B., 2011. Review of computational fluid dynamics for wind turbine wake aerodynamics. *Wind Energy* 14, 799–819.
- Schatzmann, M., Olesen, H., Franke, J., Baklanov, A., Barmas, P., Bartzis, J., Batchvarova, E., Baumann-Stanzer, K., Berkowicz, R., Borrego, C., Britter, R., Brzozowski, K., Burzynski, J., Margarida Costa, A., Carissimo, B., Dimitrova, R., Grawe, D., Goricsan, I., Gorle, C., Hellsten, A., Janour, Z., Karppinen, A., Ketzler, M., Krajcovicova, J., Leitl, B., Martilli, A., Moussiopoulos, N., Neophytou, M., Papachristodoulou, C., Papadakis, M., Piringer, M., Reisin, T., Di Sabatino, S., Sandberg, M., Schlüenzen, H., Trini-Castelli, S., 2010. Cost 732 Model Evaluation Case Studies: Approach and Results Cost Action 732 Quality Assurance and Improvement of Microscale Meteorological Models.
- Schlichting, H., 1979. *Boundary-layer Theory*, seventh ed. McGraw-Hill, New York.

- Smagorinsky, J., 1963. General circulation experiments with the primitive equations. *Mon. Weather Rev.* 91, 99–164.
- Sørensen, J.N., Shen, W.Z., Munduate, X., 1998. Analysis of wake states by a full-field actuator disc model. *Wind Energy* 1, 73–88.
- Vermeer, L.J., Sørensen, J.N., Crespo, A., 2003. Wind turbine wake aerodynamics. *Prog. Aero. Sci.* 39, 467–510.
- Vermeulen, P.E.J., 1980. An experimental analysis of wind turbine wakes. In: *Third Int. Symp. Wind Energy Syst.*, Lyngby, Denmark, pp. 431–450.
- Whale, J., Andersonb, C.G., Bareiss, R., Wagnerc, S., 2000. An experimental and numerical study of the vortex structure in the wake of a wind turbine. *J. Wind Eng. Ind. Aerod.* 84, 1–21.
- Witha, B., Steinfeld, G., Heinemann, D., 2014. Advanced turbine parameterizations in offshore LES wake simulations. In: *The 6th International Symposium on Computational Wind Engineering (CWE) 2014*, Hamburg, Germany, pp. 1–8.
- Wu, Y.T., Porté-Agel, F., 2011. Large-eddy simulation of wind-turbine wakes: evaluation of turbine parametrisations. *Boundary-Layer Meteorol.* 138, 345–366.
- Wu, Y.T., Porté-Agel, F., 2012. Atmospheric turbulence effects on wind-turbine wakes: an LES study. *Energies* 5, 5340–5362.
- Xie, S.B., Archer, C., 2014. Self-similarity and turbulence characteristics of wind turbine wakes via large-eddy simulation. *Wind Energy* 17, 657–669.
- Yousefi, I., Yamaguchi, A., Ishihara, T., 2016. The effect of control logic on wind turbine tower load. In: *WWEC2016*, pp. 1–4.